




ARTICLE

<https://doi.org/10.1038/s41467-020-16142-7>

OPEN

Homologous recombination DNA repair deficiency and PARP inhibition activity in primary triple negative breast cancer

Neha Chopra¹, Holly Tovey², Alex Pearson ¹, Ros Cutts¹, Christy Toms², Paula Proszek³, Michael Hubank³, Mitch Dowsett^{1,4}, Andrew Dodson⁴, Frances Daley¹, Divya Kriplani¹, Heidi Gevensleben¹, Helen Ruth Davies^{5,6}, Andrea Degasperi ^{5,6}, Rebecca Roylance⁷, Stephen Chan⁸, Andrew Tutt^{1,9}, Anthony Skene¹⁰, Abigail Evans¹¹, Judith M. Bliss², Serena Nik-Zainal ^{5,6} & Nicholas C. Turner^{1,12}✉

Triple negative breast cancer (TNBC) encompasses molecularly different subgroups, with a subgroup harboring evidence of defective homologous recombination (HR) DNA repair. Here, within a phase 2 window clinical trial, RIO trial (EudraCT 2014-003319-12), we investigate the activity of PARP inhibitors in 43 patients with untreated TNBC. The primary end point, decreased Ki67, occurred in 12% of TNBC. In secondary end point analyses, HR deficiency was identified in 69% of TNBC with the mutational-signature-based HRDetect assay. Cancers with HRDetect mutational signatures of HR deficiency had a functional defect in HR, assessed by impaired RAD51 foci formation on end of treatment biopsy. Following rucaparib treatment there was no association of Ki67 change with HR deficiency. In contrast, early circulating tumor DNA dynamics identified activity of rucaparib, with end of treatment ctDNA levels suppressed by rucaparib in mutation-signature HR-deficient cancers. In ad hoc analysis, rucaparib induced expression of interferon response genes in HR-deficient cancers. The majority of TNBCs have a defect in DNA repair, identifiable by mutational signature analysis, that may be targetable with PARP inhibitors.

¹Breast Cancer Now Toby Robins Research Centre, The Institute of Cancer Research, London CB2 0XZ, United Kingdom. ²Clinical Trials and Statistics Unit, The Institute of Cancer Research, London, United Kingdom. ³The Centre for Molecular Pathology, The Royal Marsden Hospital, 15 Cotswold Road, Sutton SM2 5NG Surrey, United Kingdom. ⁴Ralph Lauren Centre for Breast Cancer Research, Royal Marsden Hospital, London, United Kingdom. ⁵Department of Medical Genetics, The Clinical School, Box 238, Level 6 Addenbrooke's Treatment Centre, Cambridge Biomedical Campus, Cambridge CB2 0QQ, United Kingdom. ⁶MRC Cancer Unit, Hutchison/MRC Research Centre, University of Cambridge, Box 197, Cambridge Biomedical Campus, Cambridge CB2 0XZ, United Kingdom. ⁷University College London Hospitals NHS Foundation Trust, NIHR University College London Hospitals Biomedical Research Centre, London, United Kingdom. ⁸Nottingham University Hospital Trust (City Campus), Nottingham, United Kingdom. ⁹Breast Cancer Now Research Unit, Cancer Centre, Guy's Hospital, King's College London, London, United Kingdom. ¹⁰Royal Bournemouth Hospital, Bournemouth, United Kingdom. ¹¹Poole Hospital NHS Foundation Trust, Poole, United Kingdom. ¹²Breast Unit, The Royal Marsden Hospital, Fulham Road, London, United Kingdom. ✉email: nick.turner@icr.ac.uk

Triple negative breast cancer (TNBC) may have diverse defects in HR DNA repair, through germline mutations in *BRCA1*, *BRCA2* and *PALB2*, somatic mutations in *BRCA1* and *BRCA2*, promoter methylation of *BRCA1* and *RAD51C*, and other as yet to be identified mechanisms^{1–4}. Over the last decade, advances in whole-genome sequencing (WGS) have led to the identification of mutational processes that leave a characteristic imprint, a mutational signature on the cancer genome. These have revolutionised our understanding of cancer and has the capability to improve diagnosis and treatment of cancer^{5,6}.

Cancers with defects in HR-based DNA repair have characteristic chromosomal changes reflecting the use of alternative error-prone repair pathways, including measures of genomic instability; loss of heterozygosity, telomeric allelic imbalance and large-scale state transitions to accurately identify *BRCA1/2* tumours^{7–9}, and their combination to form the HRD Score has allowed identification of HR-deficient tumours (HRD Score >42), independent of *BRCA1/2* deficiency within a sporadic TNBC population¹⁰. Recent work has identified WGS signatures of HR deficiency with *BRCA1/2* deficient tumours associated with distinct mutational signatures. The mutational signatures and chromosomal instability markers of HR deficiency have been aggregated into the HRDetect score, robustly identifying *BRCA1/2* tumours with potential greater accuracy than indexes such as HRD-score^{11,12}.

Whether mutational signature-based scores such as HRDetect, can be used to direct therapy in the clinic is unknown, in part as

there is limited direct evidence that cancers classified as HR deficient by these scores have a functional defect in HR. Breast cancers with *BRCA1* and *BRCA2* germline mutations are highly sensitive to PARP inhibitors^{13,14}, which target the underlying HR DNA repair defect in these cancers. However, no activity was observed with PARP inhibitors in the treatment of heavily pre-treated un-selected advanced TNBC¹⁵. The extent to which this PARP inhibitor efficacy may translate to sporadic TNBC is unknown, as is the best way to identify HR-deficient TNBC. To address these questions, we designed a translational clinical trial, the RIO trial (EudraCT 2014-003319-12), with the objective of identifying biomarkers of PARP inhibitor activity in sporadic TNBC.

Results

Biomarkers of HR deficiency in primary TNBC. Patients with newly diagnosed, treatment naïve TNBC were treated with the PARP inhibitor rucaparib for 2 weeks prior to surgery or neoadjuvant chemotherapy. A total of 43 patients were entered into the trial between August 2015 and August 2017. Blood and tissue biopsies were taken prior to, and at the end of treatment, for molecular analysis (Fig. 1a). Within the trial, a subset of germline *BRCA1/2* patients were recruited as a control population. The trial prospectively examined three potential biomarkers of PARP inhibitor activity, a molecular signature of HR deficiency

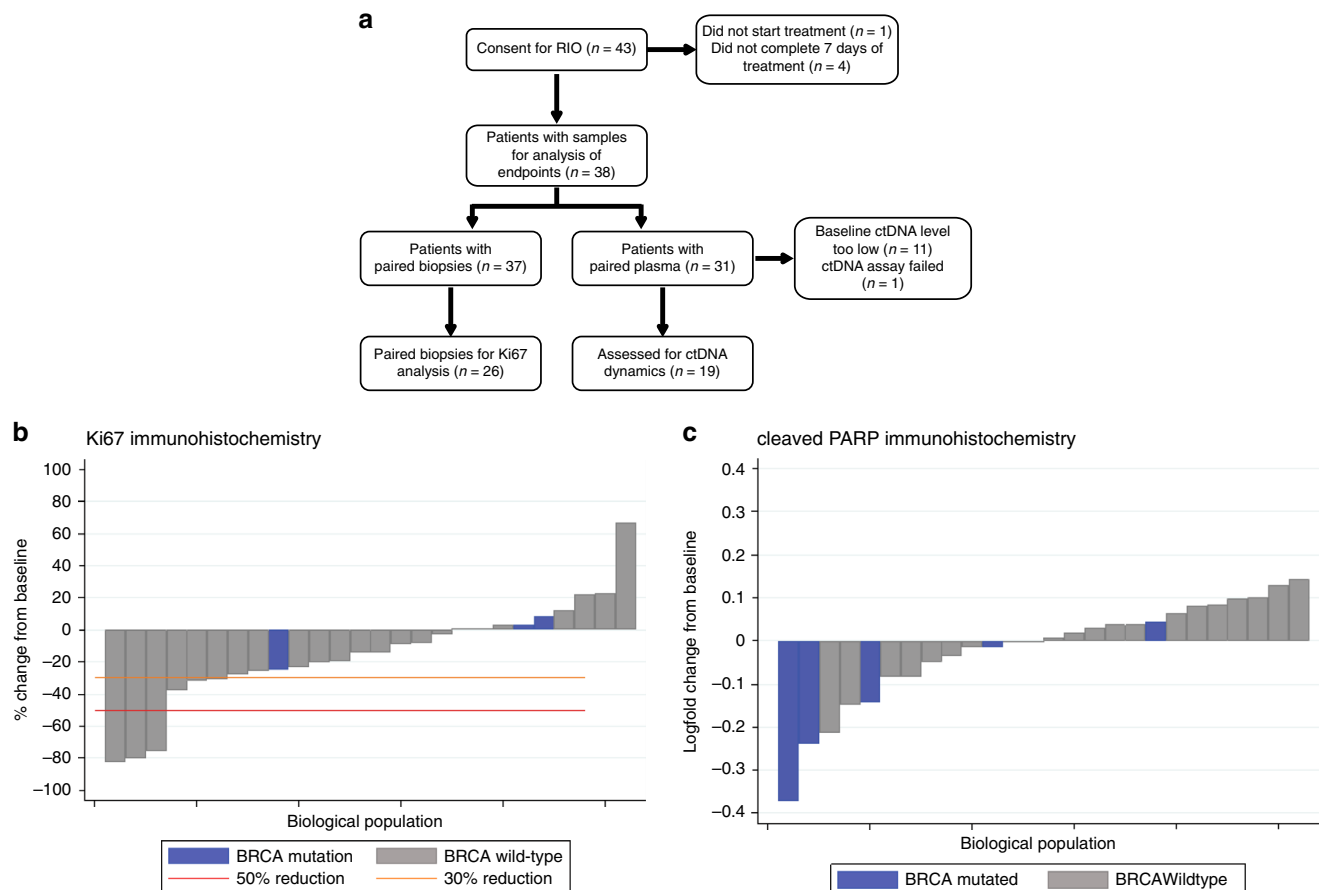


Fig. 1 RIO study CONSORT diagram and HRDetect analysis. **a** RIO study CONSORT diagram. **b** Effect of rucaparib on Ki67 expression assessed by immunohistochemistry (IHC). The change in proportion of tumor cells expressing Ki67 between baseline and EOT, in patients that had assessable pairs of baseline and EOT samples. *BRCA* mutation cancers had no evidence of decreased Ki67. **c** Effect of rucaparib on cleaved PARP expression assessed by immunohistochemistry, as a marker of apoptosis. The change in proportion of tumor cells expressing cleaved PARP between baseline and EOT, in patients that had assessable pairs of baseline and EOT samples. *BRCA* mutation cancers had no evidence of increased cleaved PARP expression. Grey bars, *BRCA* wild type patients; Blue bars, *BRCA* germline mutant patients. Orange line, >30% but <50% reduction; Red line, >50% reduction.

Table 1 RIO study patient demographics.

	<i>n</i>	%
Age (mean (standard deviation))	54.6	(13.9)
Age group (years)		
<40	7	16.3
40-49	13	30.2
50-59	9	20.9
60-69	5	11.6
70+	9	20.9
BRCA status		
Triple negative, known <i>BRCA1/2</i> carrier at registration	2	4.7
Not TN, known <i>BRCA1/2</i> mutation carrier at registration	1	2.3
Triple neg, no <i>BRCA</i> mutation	35	81.4
Triple negative, <i>BRCA1/2</i> mutation identified while on trial	5	11.6
Planned standard treatment after rucaparib		
Neoadjuvant chemotherapy	32	74.4
Hormone receptor status		
Surgical resection	11	25.6
ER & PR negative ^a	42	97.7
ER positive & PR negative	1	2.3
Tumour grade (diagnostic sample)		
G1	0	0
G2	12	27.9
G3	24	55.8
Not known	7	16.3
Histological type		
Infiltrating ductal	38	88.4
Infiltrating lobular	4	9.3
Mixed ductal & lobular	1	2.3
DCIS present		
Yes	7	16.3
No	35	81.4
Not known	1	2.3
Tumour size by ultrasound		
<1.5	2	4.7
1.5	1	2.3
>1.5 & ≤2	10	23.3
>2 & ≤5	26	60.5
>5	4	9.3
Lymph node involvement		
Yes	16	37.2
No	27	62.8
Side of tumour		
Left	18	41.9
Right	25	58.1
Evidence of metastatic disease		
Yes	0	0
No	43	100

^aOne patient was locally assessed as triple negative but central assessment noted weak PgR score of 3/8 by Allred.

using HRDetect, RAD51 focus formation in a tumor biopsy at the end of treatment, and *BRCA1* methylation. The primary activity end point was a fall in Ki67 on the end of treatment biopsy, with circulating tumor DNA dynamics as a prospectively planned exploratory end point of activity. Patient demographics were as expected for this population (Table 1). Rucaparib was well tolerated with adverse effect profile similar to previous clinical studies^{16,17} (Supplementary Table 1).

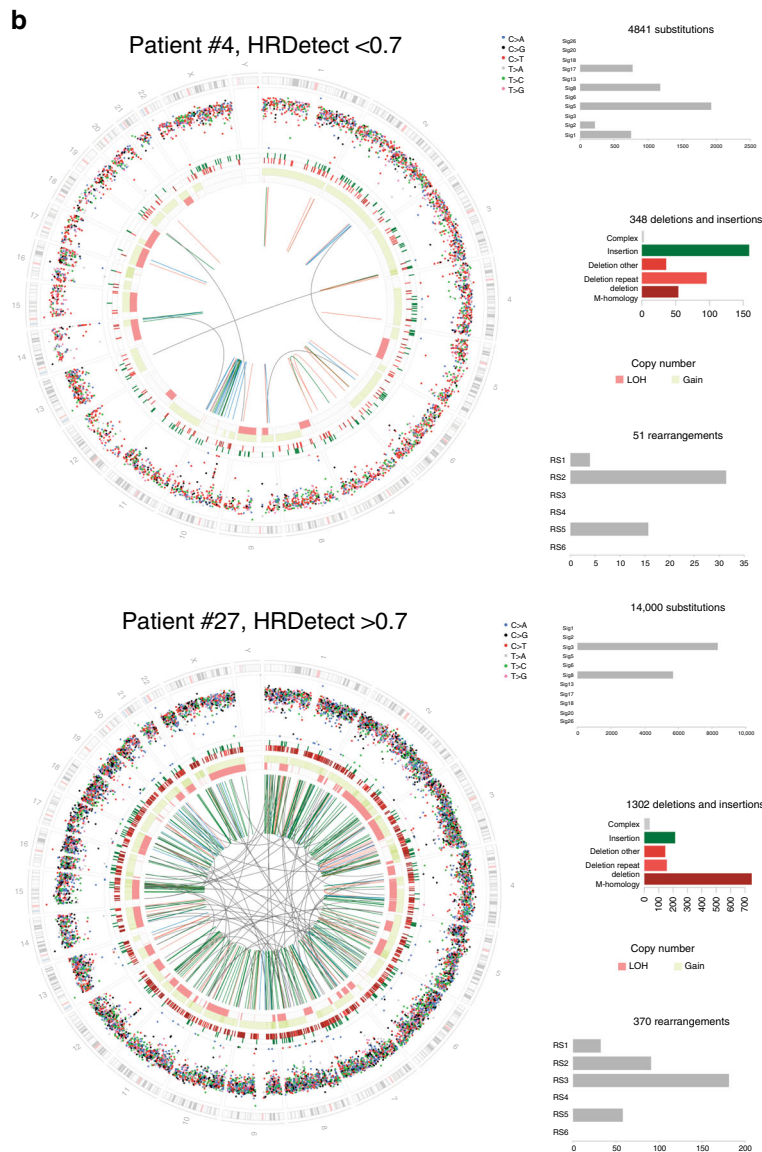
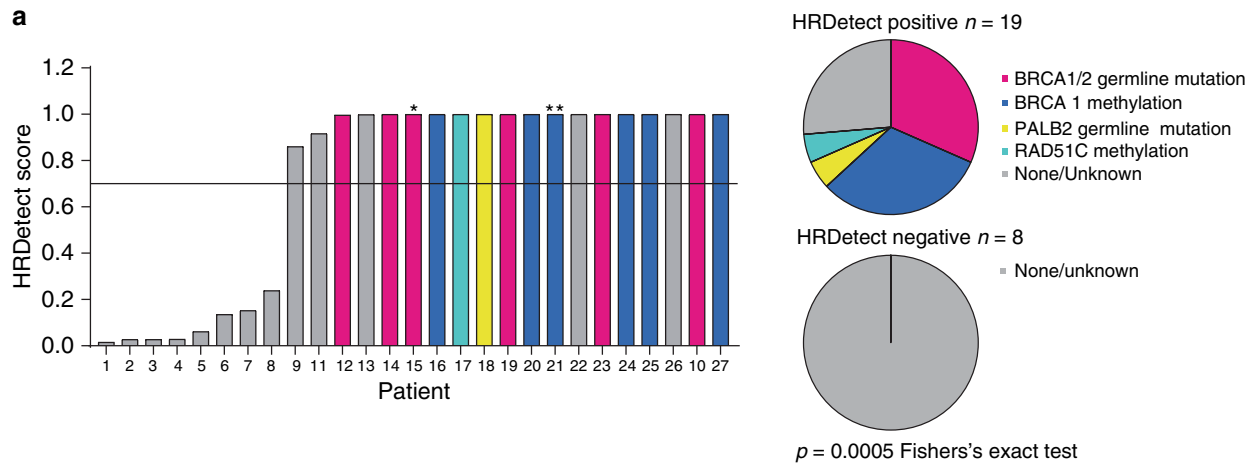
We assessed rucaparib activity and the relationship with prospectively planned biomarkers. The primary end point was assessed in tissue samples, using Ki67 suppression after two weeks assessed by immunohistochemistry, as a potential biomarker (Fig. 1b). A drop in Ki67 by 50% in the triple negative patients without a known *BRCA1/2* mutation at trial entry was seen in 12% tumors (95% CI: 2.5–31.2; $n = 3/25$). In secondary end point analysis, one additional patient with known *BRCA* mutation at

trial entry was assessed and did not have a 50% drop in Ki67 (Fig. 1b). No association was observed between Ki67 change with *BRCA1/2* mutated cancers (Fig. 1b). Similarly, no association was observed with cleaved PARP levels as a marker of apoptosis with *BRCA1/2* mutated cancers (Fig. 1c).

In secondary end point analysis, baseline biopsies of patients entering the trial, we interrogated the prevalence of HR deficiency in primary TNBC (Fig. 2 and Supplementary Table 2). We performed whole-genome sequencing analysed with the HRDetect assay¹¹, identifying mutational processes characteristic of HR deficiency in 69% locally assessed TNBC (18/26 with score >0.70, herewith called HRDetect+ve; Fig. 2a,b and Supplementary Fig. 1a) as well as an additional control ER-positive cancer with a known germline *BRCA2* mutation. In ad hoc analysis, we individually determined the mutational status of *BRCA1*, *BRCA2* and *PALB2*, and promoter methylation of *BRCA1* and *RAD51C* (Fig. 2a). Of the HRDetect+ve cancers, 74%(14/19) had a detectable underlying mutation of *BRCA1/2* and *PALB2* or gene promoter hypermethylation of *BRCA1* or *RAD51C*. None of the eight HRDetect–ve cancers had an underlying genetic/epigenetic defect ($p = 0.0005$, Fisher's exact test; Fig. 2a). A loss of heterozygosity (LOH)/copy-number-based HRD score was positive in more cancers than HRDetect, with the HRD score identifying cancers with genomic instability but without rearrangement signatures and indels at microhomology. None of the HRD score high but HRDetect low tumours had detectable pathway aberrations (Supplementary Fig. 1b), suggesting that HRDetect was more specific.

HRDetect identified all cancers with known HR pathway defects, as well as additional sporadic cancers with no single detectable defect (Fig. 2a). In secondary end point analysis, we next addressed whether HRDetect+ve cancers had an underlying functional defect in HR DNA repair, using RAD51 focus formation in the end of treatment (EOT) biopsy. When cells are exposed to genotoxic agents such as PARP inhibition, RAD51 is recruited to sites of DNA damage and stalled replication forks, mediating the search for a homologous sequence during HR¹⁸, with RAD51 nuclear foci visible at sites of repair as a hallmark for HR-mediated repair¹⁹. The impaired ability to form RAD51 foci after DNA damage may identify cancers with defective HR²⁰. We developed a novel immunohistochemistry assay to assess RAD51 foci, co-staining with geminin (GMN) to identify cells in S/G2 phase of the cell cycle and after cytotoxic treatment; RAD51 score <20% (less than 20% geminin positive cells having RAD51 foci, RAD51 foci deficiency) was assessed to indicate HR deficiency in an independent sample set (Supplementary Fig. 2). Within the RIO trial, RAD51 IHC scores increased significantly from baseline to EOT ($p = 0.0016$, Wilcoxon test), reflecting rucaparib induced DNA damage and RAD51-mediated repair (Fig. 3a). In EOT biopsies, RAD51 foci deficiency was identified in 77% (17/22) locally assessed TNBC, as well as an ER-positive *BRCA2* mutant control cancer (Fig. 3b). Of the RAD51-deficient cancers, 61% (11/18) had an underlying detectable HR defect compared to none (0/5) of RAD51 foci proficient cancers ($p = 0.037$ Fisher's exact test; Fig. 3b). Cancers with RAD51 foci deficiency had significantly higher HRDetect scores than tumour samples that were RAD51 foci proficient ($n = 18$, $p = 0.0146$ Mann–Whitney test; Fig. 3c). HRDetect therefore identified cancers with a functional defect in HR-based DNA repair, with functional HR deficiency occurring in the majority of TNBC.

Rucaparib activity assessed by ctDNA dynamics. Circulating tumour DNA (ctDNA) is released from the tumor, allowing for serial sampling through the course of treatment^{21,22}. Early changes in ctDNA dynamics represent an early biomarker of drug



activity, as cancers that respond to treatment rapidly suppress the level of ctDNA in plasma^{23–25}. Analysis of ctDNA was prospectively planned as an exploratory end point of rucaparib activity, in part, as Ki67 change has only been validated as an activity end point in endocrine based therapies^{26–28}. To assess

ctDNA in RIO, the primary tumor was sequenced in 35 patients, with somatic mutations identified in 31 patients, and personalised digital PCR used to track changes in ctDNA levels between baseline and end of treatment plasma (EOT). Change in ctDNA was assessable in the 19 patients with sufficiently high baseline

Fig. 2 HRDetect analysis. **a** HRDetect scores were established with whole-genome sequencing in baseline biopsies of 26 patients with untreated primary triple negative breast cancer (locally assessed) entering the RIO window clinical trial. HRDetect positive cancers (HRDetect score >0.7) were enriched for inactivating mutations and promoter methylation of HR genes compared to HRDetect negative cancers ($p = 0.0005$, Fisher’s exact test). Star, an additional patient with ER-positive breast cancer and *BRCA2* germline mutation is shown. 2 stars, locally assessed as TNBC but centrally assessed as PR-positive breast cancer with *BRCA1* methylation. Magenta bars, *BRCA1/2* germline mutation; Blue bars, *BRCA1* methylation; Yellow bars, *PALB2* germline mutation; Turquoise bars, *RAD51C* methylation; Grey bar, None/unknown. **b** Examples of genome plots for a sample with low (top) and high (bottom) HRDetect scores. The histograms associated with each circo plot show mutation counts for each mutation class: the topmost histogram shows the number of mutations contributing to each substitution signature; the middle histogram represents indel patterns; and the bottom histogram shows the number of rearrangements contributing to each rearrangement signature.

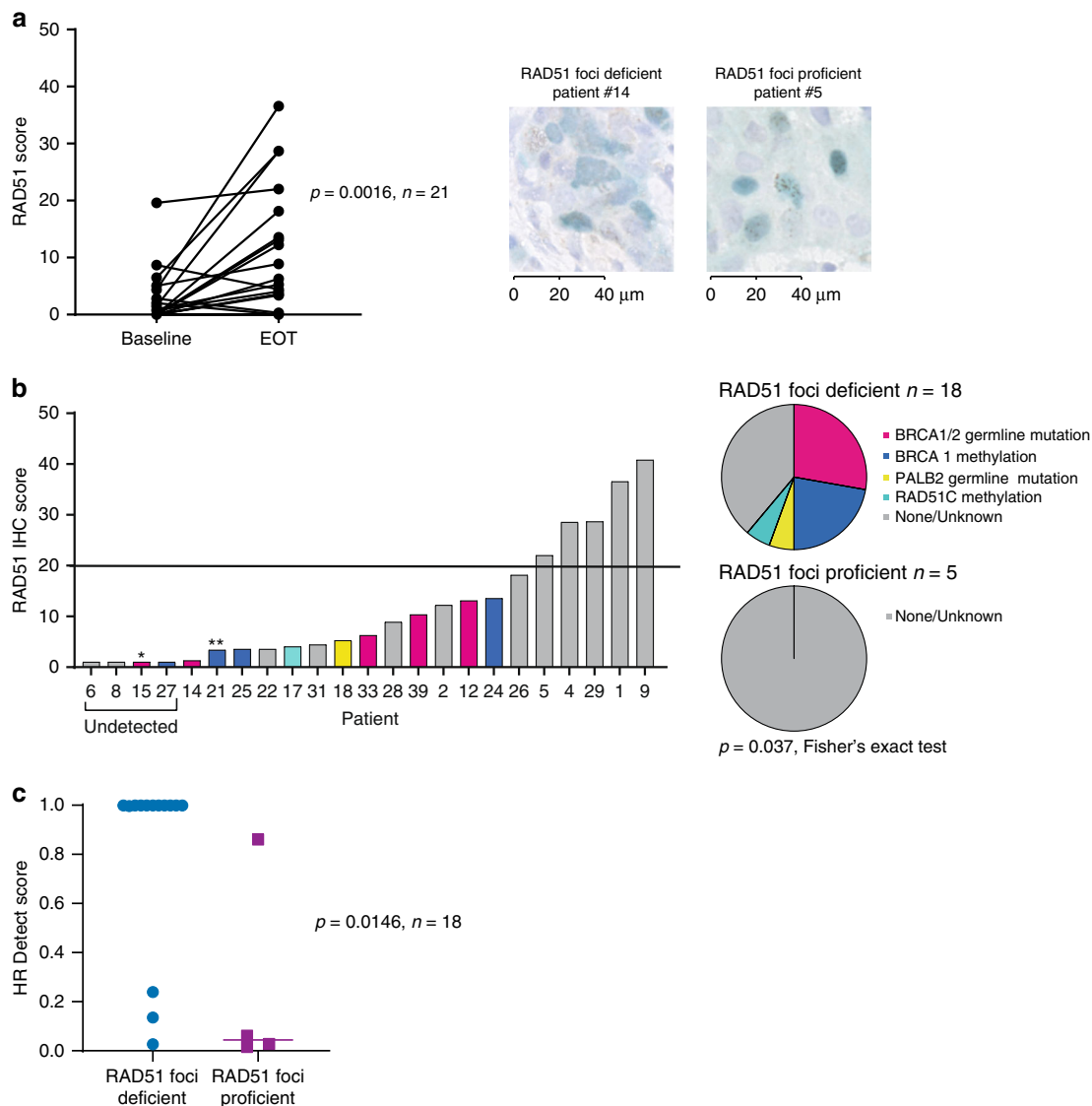


Fig. 3 Biomarkers of homologous recombination (HR) repair deficiency in TNBC. **a** RAD51 focus assessment in paired baseline and on-treatment biopsies, $p = 0.0016$ Wilcoxon test. Inset right, example immunohistochemistry images of two cancers, one deficient and one proficient in RAD51 focus formation (brown), in nuclei stained for geminin (blue). Scale bars show 40 μm . **b** RAD51 immunohistochemistry score (>20% RAD51 foci proficient), as a functional assessment of HR proficiency, was assessed in end of treatment biopsies after 2 weeks of rucaparib in 25 patients. RAD51 foci deficient cancers are enriched for inactivating mutations and promoter methylation of HR genes compared to RAD51 proficient cancers ($p = 0.037$ Fisher’s exact test). *ER-positive breast cancer and *BRCA2* germline mutation is shown. **Locally assessed TNBC but centrally assessed as PR-positive breast cancer with *BRCA1* methylation. Magenta bars, *BRCA1/2* germline mutation; Blue bars, *BRCA1* methylation; Yellow bars, *PALB2* germline mutation; Turquoise bars, *RAD51C* methylation; Grey bars, None/unknown. **c** Association between RAD51 foci proficiency and HRDetect scores in 18 patients, $p = 0.0146$ Mann-Whitney U Test. Line indicates median level.

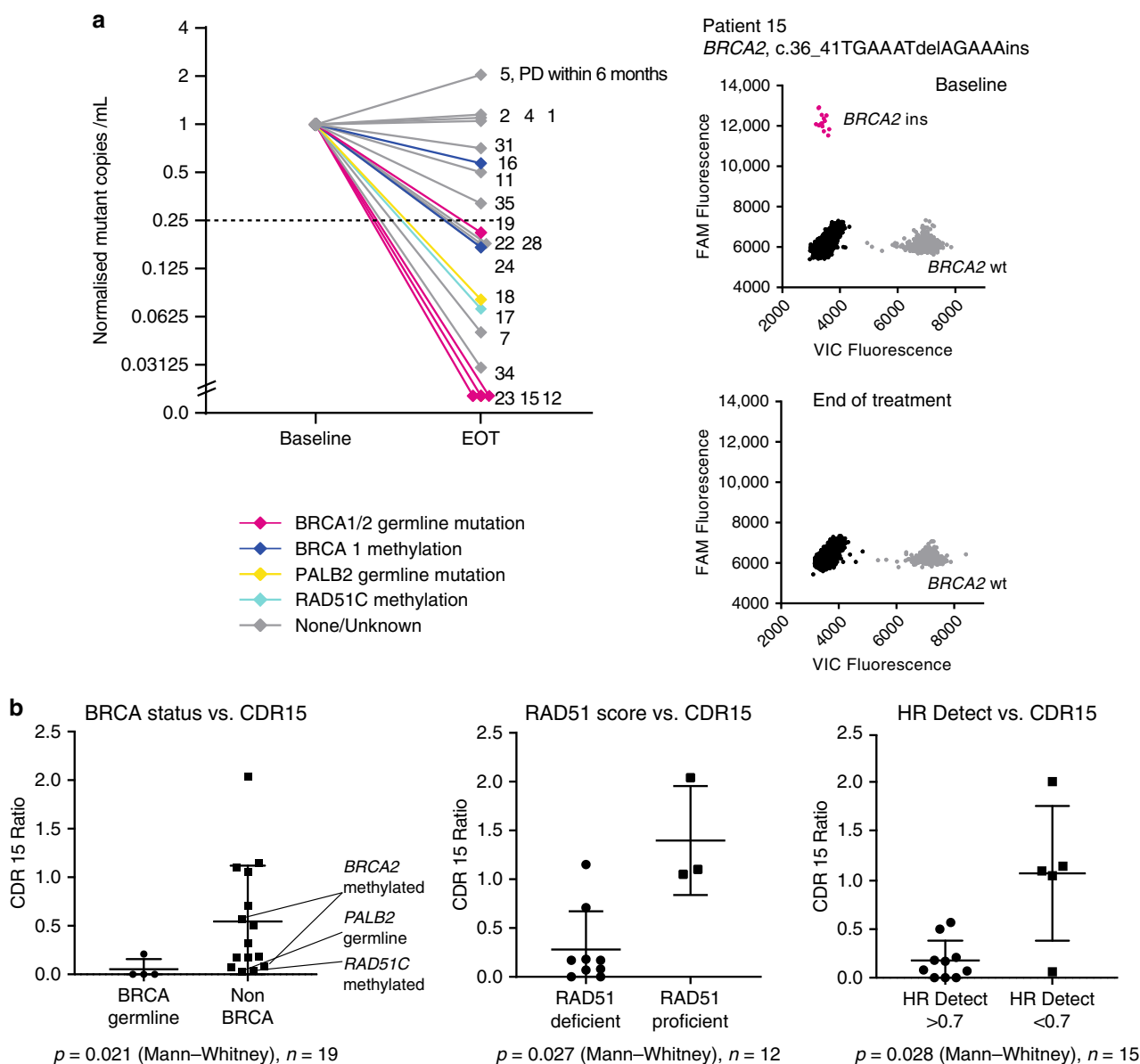


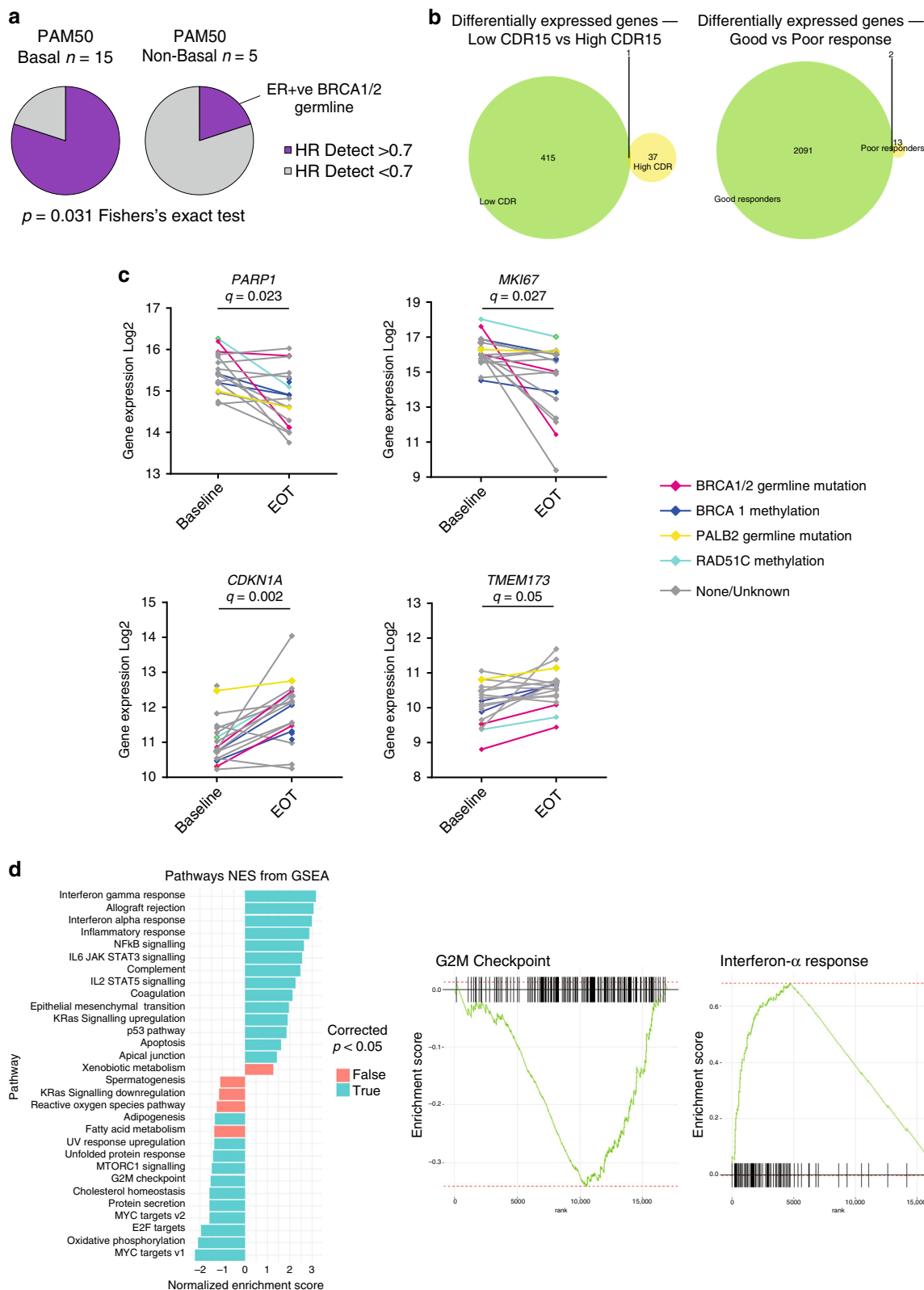
Fig. 4 ctDNA dynamics reveals activity of rucaparib in primary triple negative homologous recombination repair deficient cancers. **a** Change in circulating tumour DNA (ctDNA) copies/ml between baseline and end of treatment (EOT) after two weeks of rucaparib. The relative change of on-treatment ctDNA levels (Circulating tumor DNA ratio, CDR15) with HR pathway defects indicated. Right, example digital PCR ctDNA analysis plots. Magenta lines, *BRCA1/2* germline mutation; Blue lines, *BRCA1* methylation; Yellow lines, *PALB2* germline mutation; Turquoise lines, *RAD51C* methylation; Grey lines, None/unknown. **b** Associations of ctDNA change on rucaparib at day 15 (CDR15) with left, *BRCA1/2* germline mutations ($n = 19$ patients), middle, *RAD51* focus proficiency ($n = 12$ patients) and right, HRDetect score ($n = 15$ patients). Centre line, mean; error bars, standard deviation. p values Mann–Whitney U test.

ctDNA to assess change (Figs. 1a and 4a and Supplementary Tables 4 and 5). In contrast to the tumor biopsy-based data, a substantial proportion of patients suppressed ctDNA after rucaparib treatment (Fig. 4a).

Patients with germline *BRCA1/2* mutations did not suppress Ki67, nor induce PARP cleavage, in the end of treatment biopsy (Fig. 1). In contrast, patients with germline *BRCA1/2* mutations had a greater suppression of ctDNA than patients without germline mutations ($n = 19$, $p = 0.021$, Mann–Whitney; Fig. 4b), validating ctDNA dynamics as a marker of rucaparib activity. Cancers with deficient *RAD51* foci formation ($n = 12$, $p = 0.033$, Mann–Whitney) and HRDetect+ve cancers had greater ctDNA suppression ($n = 15$, $p = 0.027$, Mann–Whitney; Fig. 4b). In ad hoc analysis patients with suppressed ctDNA after two weeks

rucaparib (ctDNA ratio (CDR) <0.25, methods) were enriched for germline mutations of *BRCA1/2* and *PALB2* and gene promoter methylation of *BRCA1* and *RAD51C* (Fig. 4b). These data illustrate the potential of ctDNA analysis to transform window trials, presenting a simple and robust assay of drug activity, without the potential sampling challenges involved with repeat biopsies. However, analytical challenges associated with low plasma DNA levels and low purity tumor samples, will benefit from further technological development.

PARP inhibition induces an interferon response in HR-deficient cancers. Having demonstrated that HRDetect identifies sporadic TNBC in which PARP inhibitors have activity, in ad



hoc analysis we investigated the mechanisms of PARP inhibition in these cancers with RNA exome sequencing in 20 paired tumour samples, baseline and end of treatment. The majority of tumours were basal-like by PAM50 (75%, 15/20), with HRDetect scores >0.7 found in 80% (12/15) basal-like TNBC and none (0/4) of the non-basal TNBC, with one non-basal *BRCA1* mutant ER+

tumour having an HRDscore >0.7 ($p = 0.031$ Fisher's exact test, Fig. 5a). Analysis of the immune micro-environment of baseline samples with CIBERSORT²⁹ suggested higher levels of follicular helper T cells ($p = 0.0126$, $n = 20$ patients) in HRDetect+ve cancers along with higher levels of activated macrophages (Supplementary Fig. 3a and b).

Fig. 5 Expression analysis of primary triple negative homologous recombination repair deficient cancers. **a** Association between basal-like and non-basal-like triple negative subtypes, assessed by PAM50, and HRDetect score. p value Fisher's exact test. $n = 20$ paired tumour samples. Purple, HRDetect score >0.7 ; Grey, HRDetect score <0.7 . **b** Change in gene expression on paired tumor biopsies between baseline and end of treatment on rucaparib. Number of genes with a significant change in gene expression (Log fold change >0.5 and false discovery corrected q value <0.1). Left, categorised by ctDNA suppression or not (CDR15 response <0.25 vs ≥ 1 , $n = 8$ and $n = 3$ paired tumour samples respectively). Right, by CDR15 response and HRD score (CDR15 <0.25 and HRD >0.7 vs CDR15 ≥ 1 and HRD <0.7 , $n = 11$ and $n = 6$ paired tumour samples respectively). **c** Gene expression changes of *PARP1*, *MKI67*, *CDKN1A* and *TMEM173* through treatment, from DESeq2 with false discovery rate (FDR) corrected q value for change. $n = 20$ paired tumour samples. Magenta lines, *BRCA1/2* germline mutation; Blue lines, *BRCA1* methylation; Yellow lines, *PALB2* germline mutation; Turquoise lines, *RAD51C* methylation; Grey lines, None/unknown. **d** Left, Gene set enrichment pathway analysis (GSEA) for gene expression changes through treatment in patients with ctDNA suppression (CDR15 <0.25 , $n = 8$ paired tumour samples.) on rucaparib. Centre, suppression of G2M checkpoint genes on PARP inhibition, $q = 0.006$, and right, increased expression of interferon pathway genes on PARP inhibition, $q = 0.001$. False discovery rate corrected q value for change.

Cancers with ctDNA suppression (CDR <0.25) had more substantial changes in gene expression than cancers without ctDNA suppression (CDR >0.25), with 415 compared to 37 significantly differentially expressed genes respectively (Fig. 5b), demonstrating stability of gene expression through rucaparib treatment in HR-proficient cancers. For individual genes, a significant decrease in gene expression was noted in *PARP1* mRNA ($q = 0.023$, $n = 20$, DESeq2 with false discovery rate (FDR) correction), *MKI67* mRNA (*Ki67*, $q = 0.027$, $n = 20$, DESeq2 FDR correction), as well as induction in gene expression of both *CDKN1A* mRNA (*p21*, $q = 0.002$, $n = 20$, DESeq2 FDR correction) and *TMEM173* mRNA (*STING*, $q = 0.05$, $n = 20$, DESeq2 FDR correction; Fig. 5c). In HRDetect+ve cancers (Supplementary Fig. 4) and cancers with associated ctDNA suppression (Fig. 5d) pathway analysis demonstrated significant gene expression changes in pathways that regulate proliferation, apoptosis and immune function. There was decreased expression of G2M checkpoint genes, reflecting cell cycle arrest with rucaparib (Fig. 5d). There was substantial increase in interferon response genes, which along with *TMEM173* mRNA expression, suggested PARP inhibition activated the cGAS–cGAMP–STING pathway in HR-deficient cancers (Fig. 5d and Supplementary Fig. 4). In contrast, HRDetect-ve cancers did not induce interferon response genes, nor had expression changes of cell cycle arrest, on rucaparib (Supplementary Fig. 4).

Discussion

Results from the RIO trial demonstrate that a majority of primary TNBC have defects in HR-based DNA repair, reinforcing the companion population-based TNBC study by Staaf et al.⁴ The primary end point of RIO, suppression of *Ki67* in on-treatment biopsies, was infrequent. In pre-planned secondary analyses, we show that cancers with HR deficiency can be robustly identified with the mutational-signatures based classifier HRDetect (Fig. 2 and Supplementary Fig. 1), which identifies cancers with a functional deficiency in HR (Fig. 3b), and with evidence of activity of PARP inhibitors restricted to these cancers using ctDNA analysis (Fig. 3c). In ad hoc analysis, HRDetect was more specific to underlying HR deficiency than HRD scores (Supplementary Fig. 1b), suggesting that mutational signature assessment might be more accurate in identifying cancers that would benefit from platinum chemotherapy or PARP inhibition^{4,30–32}.

Induction of RAD51 nuclear foci after neoadjuvant chemotherapy and PARP inhibition can measure the homologous recombination functionality in breast cancer biopsies^{20,33–36}, with an association to loss of heterozygosity measures of HR deficiency^{34,37}. Studies have shown that cells with deficient *BRCA1/2* or other HR proteins, do not efficiently form RAD51 foci which could be used as a marker for PARP inhibitor sensitivity using FFPE tumour samples^{35,38,39}. The dynamics of DNA repair alter throughout tumour evolution and a functional RAD51 assay can be used as a dynamic readout of tumour HR status at the specific time for treatment decision-making^{33,40,41}. Current studies are using immunofluorescence (IF)

on FFPE samples which can be labour intensive, and here we develop a RAD51 foci immunohistochemistry (IHC). Our cutoff $<20\%$ for HR deficiency is consistent with the RECAP test which has recently shown to be effective in ascertaining HR deficiency in metastatic breast tumours treated with ionising radiation³⁶. Further validation of this novel HR deficient biomarker is required and if clinically validated could be a useful tool in the clinic.

One of the main limitations of the study was lower recruitment into the trial than was anticipated. This was possibly due to patient preference to start treatment without the possibility of delaying for short-term trial therapy. Additionally, failure of tissue biopsies containing enough tumour content impacted end point analysis. We therefore demonstrate the advantage of non-invasive analysis, and the use of ctDNA as a potentially reliable and effective surrogate end point to assess response. This will require further validation.

We demonstrate that PARP inhibitors induce a pro-inflammatory/interferon response in HR-deficient TNBC, likely through the cGAS–cGAMP–STING pathway. Consistent with our findings, PARP inhibition has previously been shown to induce T-cell recruitment through activation of the cGAS–cGAMP–STING pathway in a *BRCA1*-null mouse model of TNBC⁴². Similarly, PARP inhibitors have been shown to upregulate interferon response in TNBC cell lines with *BRCA2* depletion⁴³ or mutant *BRCA1*⁴⁴. Furthermore, Sceneay et al.⁴⁵ recently demonstrated using mouse models of TNBC, that immune dysfunction characterised by decreased interferon signalling and decreased antigen presentation was abrogated by a STING agonists. Together these findings underline the potential of exploiting immune dysfunction in the context of HR deficiency, notably in *BRCA1/2* mutant tumours, and TNBC more generally.

Our findings illustrate the potential of using whole-genome sequencing mutational signatures to guide cancer treatment, advocating for clinical trials of PARP inhibitors, potentially in combination with PD(L)1 targeting immune checkpoint antibodies, in sporadic TNBC with HR deficiency.

Methods

Study Design. Conducted in 10 hospitals throughout the United Kingdom, the window study of the PARP inhibitor rucaparib in patients with primary triple negative or *BRCA1/2* related breast cancer (The RIO study; EudraCT 2014-003319-12, Cancer Research UK trial CRUK/12/034) was a single-group, open-label, phase II window of opportunity trial assessing rucaparib efficacy in patients with primary triple negative or *BRCA1/2* mutant breast cancer prior to commencing primary treatment (neoadjuvant chemotherapy or surgery). The trial was co-sponsored by the Institute of Cancer Research and the Royal Marsden Hospital NHS Foundation Trust. Ethical approval for The RIO trial was given by the NRES Committee London - Fulham Research Ethics Committee (REC ID: 14/LO/2181) and informed consent was obtained from all patients enrolled in the study.

Key eligibility criteria include breast tumour size ≥ 2 or <2 cm with cytologically/histologically confirmed axillary lymph nodes, WHO performance status 0–2, no prior history of ipsilateral breast cancer within 5 years and no prior treatment with PARP inhibitors. Patients received rucaparib 600 mg twice daily for 12–14 days. Baseline bloods (EDTA and STRECK) and core biopsies (FFPE and RNAlater™) were collected at time of diagnostic biopsy or following trial entry. End of

treatment bloods (STRECK) and biopsies (FFPE and RNAlater™) were taken at surgery or prior to neo-adjuvant chemotherapy within 24–48 h of the last rucaparib dose. The primary end point was Ki67 response from baseline to end of treatment defined as a $\geq 50\%$ decrease. Secondary endpoints (pre-specified endpoints in the trial protocol) were association between baseline biomarkers of *BRCA1* methylation and a genomic predictor of HR deficiency (HRDetect) with Ki67 response to rucaparib, apoptosis induction following 12–14 days of rucaparib, the proportion of sporadic TNBC that fail to induce RAD51 foci on end of treatment biopsy (RAD51 score), safety and tolerability of rucaparib, association of biomarkers with RAD51 score, the proportion of patients with a change in circulating tumour DNA levels in response to rucaparib, association between change in circulating tumour DNA levels with biomarkers, and proportion of patients with *BRCA1* and *BRCA2* germline mutation related cancers with a Ki67 response to rucaparib and the proportion that have reduced RAD51 score and increased apoptosis induction. Pathological complete response was not assessed as an end point, as the two weeks window was considered to be too short for this end point. Where molecular analysis was not pre-specified in the trial protocol, this is highlighted as being ad hoc analysis.

Ki67 IHC and Scoring. Immunohistochemistry for Ki67 was performed and scored according to Leung et al.⁴⁶ Tissue sections were deparaffinised and rehydrated prior to antigen retrieval using low pH (pH 6.0) Target Antigen Retrieval Solution (K8005, Dako UK Ltd). Tissue sections were stained for Ki67 using mouse monoclonal anti-Ki67 antibody (MIB-1 clone, Dako, M7240) diluted 1:50 in EnVision Antibody Diluent (K8006, Dako UK Ltd). Sections were washed using wash buffer (Dako, S3006) before colour development using REAL Kit (Dako, K5001). Tissues sections were counter stained with hematoxylin and coverslips mounted using DPX. The percentage of Ki67 positive cells was calculated from between 200–400 invasive tumour cells according to the method of Leung et al.⁴⁶. A Ki67 response was determined as a $>50\%$ fall in Ki67 at EOT compared to baseline.

Cleaved PARP IHC and scoring. IHC for cleaved PARP (cPARP) was performed using a rabbit monoclonal antibody specific for PARP cleaved at Asp214. Tissue sections were deparaffinised and rehydrated prior to antigen retrieval using High pH (pH9.0) Target Antigen Retrieval Solution (K8004, Dako UK Ltd), in PT-LINK (PT101, Dako UK Ltd). Tissue sections were stained for cPARP using rabbit monoclonal anti-cPARP antibody (Asp214, clone D64E10, Cell Signaling Technology, #5625) diluted 1:100 in EnVision Antibody Diluent (K8006, Dako UK Ltd). Sections were washed using wash buffer (Dako, S3006) before colour development using anti-rabbit link reagent EnVision FLEX LINKER (K8019, Dako UK Ltd). Tissues sections were counter stained with hematoxylin and coverslips mounted using DPX. The percentage of cPARP positive cells was calculated from a minimum of 500 invasive tumour cells. If fewer than 500 invasive tumour cells were present the sample was recorded as insufficient invasive tumour (IIT).

Sample processing. All samples were processed by the central laboratory as part of the RIO trial. Fresh tumour samples were collected in RNAlater™ tubes, processed within 24 h and stored at -80°C until required for extraction. Baseline biopsies were sectioned using a cryostat. One section was cut for H&E and 16 sections were cut and stained with Nuclear Fast Red (NFR). A second H&E section was cut at the end of the series. H&E sections were reviewed and marked by a pathologist for macro-dissection. If the baseline biopsy did not have tumour the EOT biopsy (day 12–14) was used for sequencing. DNA was extracted using the Qiagen DNeasy Blood and Tissue kit according to the manufacturer's instructions. DNA was eluted into 200 μl buffer ATE and stored at -20°C before quantification. DNA was quantified on the Bio-Rad QX-200 ddPCR system running Qantasoft v1.7, using the *RPPH1* (RNaseP, cat# 4403328 ThermoFisher) reference assay to calculate copies/well and multiplying by the *c* value (3.3 pg), an estimate of the mass of a single haploid human genome.

Blood collected in STRECK preservation tubes at baseline (day 1 prior to treatment) and end of treatment were processed within 24 h of sample collection. Plasma and buffy coat was separated by centrifugation 1600g for 20 min and stored individually at -80°C until DNA extraction. For plasma extraction, up to 4mls of archived plasma was extracted using the automated MagMax Cell-Free DNA Isolation Kit (Thermo Cat # A29319) and ThermoScientific KingFisher Flex Purification System. DNA was eluted into 100 μl buffer AVE and stored at -20°C . Buffy coat extraction was performed using the Qiagen DNeasy blood and tissue kit as per manufacturer's instructions. DNA was eluted into 100 μl buffer AE and stored at -20°C . Plasma DNA was quantified on the Bio-Rad QX-200 ddPCR system using the *RPPH1* reference assay to calculate copies/well and multiplying by the *c* value (3.3 pg), an estimate of the mass of a single haploid human genome.

HRDetect Assay. Extracted DNA from fresh tissue with $>20\%$ tumour content and >200 ng quantifiable DNA, along with paired buffy coat germline DNA, were subject to whole-genome sequencing at the Sanger Institute, Cambridge, UK.

A 500-bp insert genomic libraries were constructed according to Illumina library protocols and 150 bp paired-end sequencing performed on an Illumina HiSeq X Ten using HCS (v3.5.0) for HiSeq X systems, to an average sequence depth of 38.5 \times for both tumour and normal. The resulting reads were aligned to the

reference human genome (GRCh37) using Burrows-Wheeler Aligner (BWA) (0.7.16a (r1181)). Mutation calling was performed as described previously¹². CaVEMan (Cancer Variants Through Expectation Maximization: <http://cancerit.github.io/CaVEMan/>) was used for calling somatic substitutions. Indels in the tumour and normal genomes were called using a modified Pindel version 2.0. (<http://cancerit.github.io/cgpPindel/>). Structural variants were discovered using a bespoke algorithm, BRASS (BReakpoint AnalysisIS) (<https://github.com/cancerit/BRASS>). All annotation was to Ensembl build 75. Allele-specific copy number analysis of tumours was performed using ASCAT (v2.1.1) applied to next-generation whole-genome sequencing data as described previously^{11,12}. Copy number values and estimates of aberrant tumour cell provided by ASCAT were input into the CaVEMan substitution algorithm. In addition, ASCAT segmentation profiles were used to establish the presence of copy number changes and loss of heterozygosity across the *BRCA1*, *BRCA2* and *PALB2* genes.

The predominant mutational signatures present in breast cancer have been identified in a large WGS study involving 560 breast cancers. These comprise 12 substitution signatures and 6 structural rearrangement signatures. The contributions of these consensus mutational signatures were estimated in the 27 RIO trial WGS samples as described previously^{12,47}. In addition, the contribution of small insertions and deletion at regions of micro-homology or repeats and HRD LOH index were estimated⁷.

Mutational signature contributions for substitution signatures 3 and 8, rearrangement signatures 3 and 5, deletions at microhomology and HRD LOH index were calculated for each sample as input in to the weighted model, HRDetect. The HRDetect algorithm was run as described previously, using the previously described weights¹¹.

Targeted tissue sequencing. Paired tissue and buffy coat DNA were sent to the Centre of Molecular Pathology at The Royal Marsden Hospital for sequencing using a targeted capture-based approach designed to detect mutations and amplifications frequently seen in breast cancer. The targeted panel, “ABC-Bio” panel, has been validated in the ABC-Bio (molecular screening for patients with advanced breast cancer) trial and comprises of 41 genes commonly mutated in breast cancer⁴⁸. Libraries were run on a MiSeq (Illumina) using MiSeq Reporter (MSR v2.5.1). All internally developed code is accessible on request.

AVENIO sequencing. ctDNA samples from six patients from whom adequate tumour samples were not obtained were sent to Roche for sequencing using the AVENIO ctDNA targeted tumour profiling kit (Roche Sequencing). A total of 4 samples were sequenced on the AVENIO ctDNA targeted kit (17 genes) and 2 samples were run on the AVENIO ctDNA expanded kit (77 genes), using HighOutput 300 cyc kit on a NextSeq 500 (Illumina) using NextSeq system suite (v2.2.0). Data was analysed using the AVENIO Oncology analysis software (v1.0.0 and v1.1) available from Roche.

BRCA1 and Rad51C methylation, bisulfite sequencing. The promoter region of *BRCA1* and *RAD51C* was identified using the Eukaryotic Promoter Database (<http://epd.vital-it.ch/index.php>). *BRCA1* promoter was amplified with forward-TATTTTGTAGAGGTTGCTGTTTAG and reverse-CTAAAAAACCCACAACC TATCCC primers. Analysis of *BRCA1* methylation was pre-planned, and *RAD51C* methylation was added ad hoc to *BRCA1* methylation prior to association with activity surrogates, as the potential importance of *RAD51C* methylation in TNBC was only recognised after the start of the trial². The *RAD51C* promoter was amplified with forward-TGGTAATTGGTTAGTGTGTGT and reverse-TCCTCA TCAAATATACACCTAACT primers. *BRCA1* and *RAD51C* PCR conditions were optimised for multiplex assay using ThermoFisher Scientific AccuPrime Hi-fidelity Taq. Human methylated and unmethylated DNA (Zymo Research, Human HCT116DKO non-methylated DNA and HCT116DKO methylated DNA) primers were used as a control.

Extracted DNA from RIO RNA Later samples were subjected to bisulfite sequencing (Zymo Research Methylation Gold spin column kit D5005). Total DNA input ranged from 10 to 500 ng. Samples were quantified post bisulfite sequencing using Qubit 3.0 fluorimeter and subsequently subjected to PCR using ThermoFisher Scientific AccuPrime Hi-fidelity Taq at 60°C for 34 cycles. Samples were cleaned using Qiagen QIAquick PCR purification kit (ID:28104) and quantified using Qubit 3.0 fluorimeter. Samples were subjected to Illumina NebNext Ultra II library preparation. Total library input ranged from 10–116 ng and PCR cycles were adjusted accordingly, and sequenced on the Illumina MiSeq platform with Miniseq system suite v1.1. Mean number of reads for *BRCA1* amplicon was 36909 (range 9654–60084) and *RAD51C* amplicon 48879 (range 28404–71129) with a mean 47% of reads on target for the methylation sequencing run (range 37–50%).

Bioinformatics analysis of methylation followed a similar workflow to previous studies³². Paired overlapping reads were merged into a single sequence using flash⁴⁹ after adaptor trimming using trim-galore (https://www.bioinformatics.babraham.ac.uk/projects/trim_galore/). Each read was aligned using pairwise alignment to the *BRCA1* or *RAD51C* amplicons using Biostrings R⁵⁰ package with 90% identity. Reads with more than 1 mismatch in alignment were additionally removed. Reads with incomplete bisulphite conversion were removed by

calculating the unconverted cytosine count at non CG sites as well as reads where all CG sites in the read were not C or T. Reads were assessed as being methylated when >90% of CpG sites in the amplicon were methylated. For RAD51C methylation, 2 sites in the RAD51C amplicon were removed as these were found to be consistently methylated in all samples.

Immunohistochemistry for RAD51/Geminin (GMNN) double staining. FFPE samples taken 24–48 h after the last dose of rucaparib were cut, deparaffinised, rehydrated and stained with hematoxylin and eosin (H&E) and double stained with GMNN and RAD51. Pre- and post-radiotherapy-induced squamous cell carcinoma were used as negative and positive controls.

Antigen retrieval was performed and RAD51 primary antibody (mouse monoclonal, Genetex, GTX70230) was diluted 1/200 in Dako antibody diluent (K8006) and applied. Slides were incubated with Dako Envision Flex HRP (K8002). Geminin (GMNN) antibody (rabbit polyclonal, Proteintech 10802-1-AP) diluted 1/1500 in Dako antibody diluent was applied and incubated with Dako Envision Flex HRP (K8002). Sections incubated with Vector TMB blue (SK4400) and counterstained with Gills 1 hematoxylin, air dried and dehydrated in xylene before mounted and cover slipped with Vectamount.

Five random fields at 40× magnification were identified and marked in PathXL. GMNN staining was identified with blue/green staining and RAD51 was identified by the presence of brown nuclear foci. Scoring was done by 2 scorers blinded to each other, time point and clinical details.

The number of tumour cells, GMNN-positive cells and RAD51-positive cells were counted. Cells with 5 or more RAD51 foci were classified as RAD51 positive. A minimum of 300 tumour cells and 30 GMNN-positive cells were a minimum requirement for inclusion. Raw data were collected and the proliferation fraction ((no. of GMNN-positive cells / total number of tumour cells) × 100) and RAD51 score ((no. of RAD51-positive cells / no. of GMNN-positive cells) × 100) was calculated.

Circulating tumor DNA analysis. For each trial subject, dPCR assays were designed for the mutations identified by tissue sequencing according to the method of Garcia-Murillas et al²². Assays were optimised with temperature gradients and patients with more than one mutation had multiplex assays optimised. If optimisation was not achieved with multiplexes, a singleplex assay was used.

Mutation analysis was done using ddPCR assays specific for each patient's mutation(s) on a QX200 system (Bio-Rad) running Quantasoft v1.7. 50 µl DNA (2 ml plasma equivalent) was used divided equally into 2 wells from each time point. DNA was dried at 60 degrees for 100 min before preparing the PCR reactions to a volume of 20 µl. Three NTCs and a negative control of the patient's buffy coat DNA were included for each dPCR assay. Only paired samples with at least 4 positive droplets in baseline samples were analysed for change in ctDNA levels. The circulating DNA ratio at day 15 (CDR15) was assessed as a ratio of the ctDNA copies/ml at EOT copies/ml compared to ctDNA copies/ml at baseline. Where more than one mutation was tracked a weighted mean of ctDNA change was calculated.

The CDR15 cutoff <0.25 for ctDNA suppression, was pre-specified determined in a separate study in metastatic breast cancer, that validated this cutoff to predict progression free survival on cytotoxic paclitaxel therapy²⁵.

RNA sequencing. Paired RNAlater™ samples were identified and sectioned using a cryostat. One section was cut for H&E and 10 sections were cut and stained with nuclease-free Nuclear Fast Red. A second H&E section was cut at the end of the series. H&E sections were reviewed and marked by a pathologist for tumour and assessed for tumour content. NFR stained sections were micro-dissected and RNA was extracted using the Qiagen RNeasy Mini kit according to the manufacturer's instructions. RNA was eluted twice into separate 50 µl RNA free water and stored at -80°C before quantification. RNA was quantified using Qubit 3.0 fluorimeter using the Qubit™ RNA HS Assay Kit (Q32852, ThermoFisher Scientific).

Extracted RNA (~1 µg) was sent to Eurofins Genetic Services Limited for RNA Exome sequencing. Total RNA was subjected to RiboZero depletion and Illumina TruSeq RNA Exome library preparation. Libraries were pooled and sequenced on an Illumina HiSeq 2500 (v4 chemistry) running HiSeq Control Software (HCS) v2.2.68. Samples were aligned to the GCh37 genome using STAR aligner (<https://github.com/alexdobin/STAR>)⁵¹ with a mean of 44,117,169 reads per sample (range 14010752-91,470,225). Gene counts were established using htseq (<https://github.com/simon-anders/htseq>)⁵². DeSeq2 (<https://doi.org/10.18129/B9.bioc.DESeq2>)⁵³ was used to establish gene-wise normalisation and to look for differential expression between different sample groups. Gene set enrichment analysis was carried out using the R package fgsea (<https://doi.org/10.18129/B9.bioc.fgsea>)⁵⁴. PAM50 and TNBC subtypes were established using AIMS (<https://doi.org/10.18129/B9.bioc.AIMS>)⁵⁵ and TNBCtype (<http://cbc.mc.vanderbilt.edu/tNBC/>)⁵⁶. Cibersort (<https://cibersort.stanford.edu/index.php>)²⁹ was run in absolute mode using normalized gene counts.

Statistics. The study size was determined using a Simon two stage Minimax design on Ki67 response in patients with sporadic TNBC, with p0 = 10% and p1 = 25% Ki67 response rate. With a two-sided alpha 1.6% and 90% power, four Ki67

responders were required in the first 41 assessable patients to proceed to a full 73 patients. The study would declare inefficacy if <4/41 or <14/73 responses were observed. An initial futility assessment was also planned after 20 evaluable patients had completed rucaparib treatment and consideration would be given to stopping the trial if 0 responses were observed. Additionally, 5, 1.6 and 1.6% two-sided alphas were allocated to assess rucaparib activity within BRCA1 methylated tumours, RAD51 foci formation tumours, and genomic classifier HRDetect tumours respectively, for a total study two-sided alpha of 10%. Up to 20 patients with known BRCA1 or BRCA2 pathogenic germline mutations at the time of trial entry were recruited as controls for exploratory determination of biomarker endpoints. The study closed to new patients after 43 patients had been recruited on advice of the IDMC (Fig. 1) due to low recruitment.

Analysis of response data was performed on patients who had taken rucaparib for 7 days or more. Safety and tolerability are assessed in all patients who received at least one dose of rucaparib. Response rates and proportions are reported with 95% confidence intervals. Associations between biomarkers are analysed using Fisher's exact test or Mann–Whitney as appropriate. Change in biomarkers between baseline and day12–14 samples are analysed using the Wilcoxon signed rank test. Analyses were conducted in Stata v13 and GraphPad Prism, with all analyses reported two-sided.

Reporting summary. Further information on research design is available in the Nature Research Reporting Summary linked to this article.

Data availability

Sequencing data from whole-genome sequencing, exome RNA seq, and targeted sequencing from tumour samples that support the findings of this study (Figs. 1–5 and Supplementary Fig. 1, 3 and 4) is deposited in the European Genome-phenome Archive (EGA), reference EGAS00001004405 <https://ega-archive.org>.

Code availability

The code used for the analysis of sequencing data is detailed here with links and references where appropriate.

Whole-genome sequencing: CaVEMan (Cancer Variants Through Expectation Maximization: <http://cancerit.github.io/CaVEMan/>), Pindel version 2.0. (<http://cancerit.github.io/cgpPindel/>), BRASS (BReakpoint AnalySiS) (<https://github.com/cancerit/BRASS>), and ASCAT (v2.1.1). Annotation was to Ensembl build 75. Code for targeted tumour sequencing is available upon request. AVENIO ctDNA sequencing: AVENIO Oncology analysis software (v1.0.0 and v1.1) available from Roche. Bisulfite sequencing: Eukaryotic Promoter Database (<http://epd.vital-it.ch/index.php>), trim-galore (https://www.bioinformatics.babraham.ac.uk/projects/trim_galore/), Biostrings R package. RNA sequencing: STAR aligner (<https://github.com/alexdobin/STAR>), htseq (<https://github.com/simon-anders/htseq>), DeSeq2 (<https://doi.org/10.18129/B9.bioc.DESeq2>), fgsea (<https://doi.org/10.18129/B9.bioc.fgsea>), AIMS (<https://doi.org/10.18129/B9.bioc.AIMS>), TNBCtype (<http://cbc.mc.vanderbilt.edu/tNBC/>) and Cibersort (<https://cibersort.stanford.edu/index.php>).

Received: 18 July 2019; Accepted: 3 April 2020;

Published online: 29 May 2020

References

- Nik-Zainal, S. & Morganella, S. Mutational signatures in breast cancer: the problem at the DNA level. *Clin. Cancer Res.* **23**, 2617–2629 (2017).
- Polak, P. et al. A mutational signature reveals alterations underlying deficient homologous recombination repair in breast cancer. *Nat. Genet.* **49**, 1476–1486 (2017).
- Turner, N. C. Signatures of DNA-repair deficiencies in breast cancer. *The N. Engl. J. Med.* **377**, 2490–2492 (2017).
- Staa, J. et al. Whole-genome sequencing of triple-negative breast cancers in a population-based clinical study. *Nat. Med.* **25**, 1526–1533 (2019).
- Nik-Zainal, S. et al. Mutational processes molding the genomes of 21 breast cancers. *Cell* **149**, 979–993 (2012).
- Alexandrov, L. B. et al. Signatures of mutational processes in human cancer. *Nature* **500**, 415–421 (2013).
- Abkevich, V. et al. Patterns of genomic loss of heterozygosity predict homologous recombination repair defects in epithelial ovarian cancer. *Br. J. Cancer* **107**, 1776–1782 (2012).
- Birkbak, N. J. et al. Telomeric allelic imbalance indicates defective DNA repair and sensitivity to DNA-damaging agents. *Cancer Discov.* **2**, 366–375 (2012).
- Popova, T. et al. Ploidy and large-scale genomic instability consistently identify basal-like breast carcinomas with BRCA1/2 inactivation. *Cancer Res.* **72**, 5454–5462 (2012).

10. Telli, M. L. et al. Homologous recombination deficiency (hrd) score predicts response to platinum-containing neoadjuvant chemotherapy in patients with triple-negative breast cancer. *Clin. Cancer Res.* **22**, 3764–3773 (2016).
11. Davies, H. et al. HRDetect is a predictor of BRCA1 and BRCA2 deficiency based on mutational signatures. *Nat. Med.* **23**, 517–525 (2017).
12. Nik-Zainal, S. et al. Landscape of somatic mutations in 560 breast cancer whole-genome sequences. *Nature* **534**, 47–54 (2016).
13. Robson, M., Goessl, C. & Domchek, S. Olaparib for metastatic germline BRCA-mutated breast cancer. *N. Engl. J. Med.* **377**, 1792–1793 (2017).
14. Litton, J. K. et al. Talazoparib in patients with advanced breast cancer and a germline BRCA Mutation. *N. Engl. J. Med.* **379**, 753–763 (2018).
15. Gelmon, K. A. et al. Olaparib in patients with recurrent high-grade serous or poorly differentiated ovarian carcinoma or triple-negative breast cancer: a phase 2, multicentre, open-label, non-randomised study. *Lancet Oncol.* **12**, 852–861 (2011).
16. Swisher, E. M. et al. Rucaparib in relapsed, platinum-sensitive high-grade ovarian carcinoma (ARIEL2 Part 1): an international, multicentre, open-label, phase 2 trial. *Lancet Oncol.* **18**, 75–87 (2017).
17. Wilson, R. H. et al. A phase I study of intravenous and oral rucaparib in combination with chemotherapy in patients with advanced solid tumours. *Br. J. Cancer* **116**, 884–892 (2017).
18. Vispe, S., Cazaux, C., Lesca, C. & Defais, M. Overexpression of Rad51 protein stimulates homologous recombination and increases resistance of mammalian cells to ionizing radiation. *Nucleic Acids Res.* **26**, 2859–2864 (1998).
19. Tashiro, S. et al. S phase specific formation of the human Rad51 protein nuclear foci in lymphocytes. *Oncogene* **12**, 2165–2170 (1996).
20. Graeser, M. et al. A marker of homologous recombination predicts pathologic complete response to neoadjuvant chemotherapy in primary breast cancer. *Clin. Cancer Res.* **16**, 6159–6168 (2010). [pii].
21. Olsson, E. et al. Serial monitoring of circulating tumor DNA in patients with primary breast cancer for detection of occult metastatic disease. *EMBO Mol. Med.* **7**, 1034–1047 (2015).
22. Garcia-Murillas, I. et al. Mutation tracking in circulating tumor DNA predicts relapse in early breast cancer. *Sci. Transl. Med.* **7**, 302ra133, <https://doi.org/10.1126/scitranslmed.aab0021> (2015).
23. Fribbens, C. et al. Tracking evolution of aromatase inhibitor resistance with circulating tumour DNA analysis in metastatic breast cancer. *Ann. Oncol.* **29**, 145–153 (2018).
24. O’Leary, B. et al. Early circulating tumor DNA dynamics and clonal selection with palbociclib and fulvestrant for breast cancer. *Nat. Commun.* **9**, 896, <https://doi.org/10.1038/s41467-018-03215-x> (2018).
25. Hrebien, S. et al. Early ctDNA dynamics as a surrogate for progression-free survival in advanced breast cancer in the BEECH trial. *Ann. Oncol.* **30**, 945–952 (2019).
26. Chang, J. et al. Biologic markers as predictors of clinical outcome from systemic therapy for primary operable breast cancer. *J. Clin. Oncol.* **17**, 3058–3063 (1999).
27. Dowsett, M. et al. Proliferation and apoptosis as markers of benefit in neoadjuvant endocrine therapy of breast cancer. *Clin. Cancer Res.* **12**, 1024s–1030s (2006).
28. Harper-Wynne, C. L. et al. Comparison of the systemic and intratumoral effects of tamoxifen and the aromatase inhibitor vorozole in postmenopausal patients with primary breast cancer. *J. Clin. Oncol.* **20**, 1026–1035 (2002).
29. Newman, A. M. et al. Robust enumeration of cell subsets from tissue expression profiles. *Nat. Methods* **12**, 453–457 (2015).
30. Telli, M. L. et al. Phase II study of gemcitabine, carboplatin, and iniparib as neoadjuvant therapy for triple-negative and BRCA1/2 mutation-associated breast cancer with assessment of a tumor-based measure of genomic instability: PrECOG 0105. *J. Clin. Oncol.* **33**, 1895–1901 (2015).
31. Isakoff, S. J. et al. TBCRC009: a Multicenter Phase II Clinical Trial of Platinum Monotherapy With Biomarker Assessment in Metastatic Triple-Negative Breast Cancer. *J. Clin. Oncol.* **33**, 1902–1909 (2015).
32. Tutt, A. et al. Carboplatin in BRCA1/2-mutated and triple-negative breast cancer BRCAness subgroups: the TNT Trial. *Nat. Med.* **24**, 628–637 (2018).
33. Naipal, K. A. et al. Functional ex vivo assay to select homologous recombination-deficient breast tumors for PARP inhibitor treatment. *Clin. Cancer Res.* **20**, 4816–4826 (2014).
34. Castroviejo-Bermejo, M. et al. A RAD51 assay feasible in routine tumor samples calls PARP inhibitor response beyond BRCA mutation. *EMBO Mol. Med.* <https://doi.org/10.15252/emmm.201809172> (2018).
35. Cruz, C. et al. RAD51 foci as a functional biomarker of homologous recombination repair and PARP inhibitor resistance in germline BRCA-mutated breast cancer. *Ann. Oncol.* **29**, 1203–1210 (2018).
36. Meijer, T. G. et al. Direct ex vivo observation of homologous recombination defect reversal after dna-damaging chemotherapy in patients with metastatic breast cancer. *JCO Precis. Oncol.* **3**, 112, <https://doi.org/10.1200/Po.18.00268> (2019).
37. Mutter, R. W. et al. Bi-allelic alterations in DNA repair genes underpin homologous recombination DNA repair defects in breast cancer. *J. Pathol.* **242**, 165–177 (2017).
38. Farmer, H. et al. Targeting the DNA repair defect in BRCA mutant cells as a therapeutic strategy. *Nature* **434**, 917–921 (2005).
39. Bryant, H. E. et al. Specific killing of BRCA2-deficient tumours with inhibitors of poly(ADP-ribose) polymerase. *Nature* **434**, 913–917 (2005).
40. Watkins, J. A., Irshad, S., Grigoriadis, A. & Tutt, A. N. Genomic scars as biomarkers of homologous recombination deficiency and drug response in breast and ovarian cancers. *Breast Cancer Res.* **16**, 211 (2014).
41. Li, X. & Heyer, W. D. Homologous recombination in DNA repair and DNA damage tolerance. *Cell Res.* **18**, 99–113 (2008).
42. Pantelidou, C. et al. PARP Inhibitor Efficacy Depends on CD8(+) T-cell recruitment via intratumoral STING pathway activation in BRCA-deficient models of triple-negative breast cancer. *Cancer Discov.* **9**, 722–737 (2019).
43. Reislander, T. et al. BRCA2 abrogation triggers innate immune responses potentiated by treatment with PARP inhibitors. *Nat. Commun.* **10**, 3143 (2019).
44. Chabanon, R. M. et al. PARP inhibition enhances tumor cell-intrinsic immunity in ERCC1-deficient non-small cell lung cancer. *The J. Clin. Invest.* **129**, 1211–1228 (2019).
45. Sceneay, J. et al. Interferon signaling is diminished with age and is associated with immune checkpoint blockade efficacy in triple-negative breast. *Cancer Cancer Discov.* **9**, 1208–1227 (2019).
46. Leung, S. C. Y. et al. Analytical validation of a standardized scoring protocol for Ki67: phase 3 of an international multicenter collaboration. *NPJ Breast Cancer* **2**, 16014, <https://doi.org/10.1038/npjbcancer.2016.14> (2016).
47. Davies, H. et al. Whole-genome sequencing reveals breast cancers with mismatch repair deficiency. *Cancer Res.* **77**, 4755–4762 (2017).
48. Pearson, A. et al. Inactivating NF1 mutations are enriched in advanced breast cancer and contribute to endocrine therapy resistance. *Clin. Cancer Res.* <https://doi.org/10.1158/1078-0432.CCR-18-4044> (2019).
49. Magoc, T. & Salzberg, S. L. FLASH: fast length adjustment of short reads to improve genome assemblies. *Bioinformatics* **27**, 2957–2963 (2011).
50. Pagès, H., Aboyoun, P., Gentleman, R. & DebRoy, S. Biostrings: efficient manipulation of biological strings. <https://rdrr.io/bioc/Biostrings/> (2019).
51. Dobin, A. et al. STAR: ultrafast universal RNA-seq aligner. *Bioinformatics* **29**, 15–21 (2013).
52. Anders, S., Pyl, P. T. & Huber, W. HTSeq—a Python framework to work with high-throughput sequencing data. *Bioinformatics* **31**, 166–169 (2015).
53. Love, M. I., Huber, W. & Anders, S. Moderated estimation of fold change and dispersion for RNA-seq data with DESeq2. *Genome Biol.* **15**, 550, <https://doi.org/10.1186/s13059-014-0550-8> (2014).
54. Sergushichev, A. An algorithm for fast preranked gene set enrichment analysis using cumulative statistic calculation. *BioRxiv* 060012 (2016).
55. Paquet, E. R. & Hallett, M. T. Absolute assignment of breast cancer intrinsic molecular subtype. *J. Natl Cancer Inst.* **107**, 357, <https://doi.org/10.1093/jnci/dju357> (2015).
56. Chen, X. et al. TNBCtype: A Subtyping Tool for Triple-Negative Breast Cancer. *Cancer Inform.* **11**, 147–156 (2012).

Acknowledgements

This study was funded by the Cridlan Trust, Clovis Oncology Inc., Cancer Research UK (CRUK; CRUK Ref A15777) core funding to the ICR Clinical Trials and Statistics Unit, Breast Cancer Now to the Breast Cancer Now Research Centre at The Institute of Cancer Research, and NHS funding to the NIHR Royal Marsden Biomedical Research Centre. HRD is funded by a CRUK Grand Challenge Award (C38317/A24043). AD is funded by a CRUK Pioneer Award. We acknowledge the assistance Katy Jarman, Lynsey Houlton, Vera Martins, Arjun Naginlal Modi. Sequencing, genomic analyses and personal funding of SNZ was supported by the Wellcome Trust Intermediate Clinical Fellowship (WT100183MA), Wellcome Beit Prize, CRUK Advanced Clinician Scientist award (C60100/A23916) and CRUK Pioneer Award.

Author contributions

N.T. conceived the RIO trial and was the chief investigator. N.T., J.B., C.T., M.D. A.T. and A.S. formed the RIO protocol development group refining the design. JB oversaw trial conduct in ICR-CTSU, statistical analysis and data interpretation. N.C. and A.P. designed and performed translation studies. H.T. and R.C. performed statistical and bioinformatics analyses. C.T. was RIO study senior trial manager. P.P. and M.H. performed targeted next-generation sequencing experiments. A.D. and F.D. performed immunohistochemistry experiments. D.K. and H.G. provided pathology support and

analysed immunohistochemistry. H.R.D., A.D. and S.N.Z. performed whole-genome sequencing and HRDetect analysis. R.R., S.C., A.T., A.S., and A.E. were principal investigators at trial sites. N.T., N.C. and A.P. wrote the manuscript and all authors contributed comments and corrections.

Competing interests

N.T., J.M.B., H.T. and C.T. report research grants and non-financial support in the form of study drug provision and distribution from Clovis Oncology Inc., during the conduct of the study. N.T. reports advisory board Honoraria from AstraZeneca, Bristol-Myers Squibb, Lilly, Merck Sharpe and Dohme, Novartis, Pfizer, Roche/Genentech, Tesaro, Bicycle Therapeutics and research funding from Astra Zeneca, BioRad, Pfizer, Roche/Genentech and Guardant Health, outside the submitted work. J.M.B. reports grants and non-financial support from AstraZeneca, Merck Sharpe & Dohme, Puma Biotechnology and Janssen-Cilag, grants, non-financial support and travel support from Pfizer and grants from Medivation, Novartis and Roche outside the submitted work. M.H. reports Honoraria or research funding from Boehringer Ingelheim, Roche Diagnostics, Bristol Myers Squibb, Guardant Health, Celgene, Eli Lilly outside of the submitted work. R.R. reports Honorarium from Pfizer. A.T. reports benefits from ICR's Inventors Scheme associated with patents for one of the PARP inhibitors in BRCA1/2 associated cancers. A.T. also reports Honoraria from Pfizer, Vertex, Prime Oncology, Artios, honoraria and stock in InBiomotion, honoraria and financial support from AstraZeneca, Medivation, Myriad Genetics, Merck Serono. S.N.Z. and H.D. are inventors on a patent application (WO2017191074A1) for HRDetect. S.N.Z. reports advisory board honoraria from Astra Zeneca and Artios Pharma. M.D. reports advisory board Honoraria from GTx, Radius, Orion and GItherapeutics, lectures fees from Myriad and Nanostring, research funding from Pfizer and Radius and income from the Institute of Cancer Research's Rewards for Inventors Scheme (Abiraterone) outside the submitted work. All other authors declare no competing interests.

Additional information

Supplementary information is available for this paper at <https://doi.org/10.1038/s41467-020-16142-7>.

Correspondence and requests for materials should be addressed to N.C.T.

Peer review information *Nature Communications* thanks the anonymous reviewers for their contribution to the peer review of this work

Reprints and permission information is available at <http://www.nature.com/reprints>

Publisher's note Springer Nature remains neutral with regard to jurisdictional claims in published maps and institutional affiliations.



Open Access This article is licensed under a Creative Commons Attribution 4.0 International License, which permits use, sharing, adaptation, distribution and reproduction in any medium or format, as long as you give appropriate credit to the original author(s) and the source, provide a link to the Creative Commons license, and indicate if changes were made. The images or other third party material in this article are included in the article's Creative Commons license, unless indicated otherwise in a credit line to the material. If material is not included in the article's Creative Commons license and your intended use is not permitted by statutory regulation or exceeds the permitted use, you will need to obtain permission directly from the copyright holder. To view a copy of this license, visit <http://creativecommons.org/licenses/by/4.0/>.

© The Author(s) 2020